Electronic Supplementary Material (ESI) for Journal of Materials Chemistry A.
This journal is © The Royal Society of Chemistry 2021

Supporting Information

Phase and Morphology Engineering of Porous Cobalt-Copper Sulfide as Bifunctional Oxygen Electrode for Rechargeable Zn-Air Battery

Linzhou Zhuang[a,1], Haolan Tao [a,1], Fang Xu [a,1], Cheng Lian [a], Honglai Liu [a], Keyu Wang [a], Jiankun Li [a], Wei Zhou [b, *], Zhi Xu [a, *], Zongping Shao [b] and Zhonghua Zhu [c]

[a] School of Chemical Engineering, East China University of Science and Technology, Shanghai, 200237, China;

[b] State Key Laboratory of Materials-Oriented Chemical Engineering, College of Chemical Engineering, Nanjing Tech University, Nanjing, 211800, China

[c] School of Chemical Engineering, The University of Queensland, Brisbane, 4072 Australia

[1] These authors contributed equally

Corresponding Authors:

* zhouwei1982@njtech.edu.cn (W. Zhou)

* zhixu@ecust.edu.cn (Z. Xu)

S1 Experimental details

S1.1 Materials

Ruthenium (IV) oxide (RuO_2, 99.9%), cobalt (II) nitrate hexahydrate ($Co(NO_3)_2·6H_2O$, ≥98%), copper (II) nitrate trihydrate ($Cu(NO_3)_2·3H_2O$, ≥99%), sodium borohydride ($NaBH_4$, ≥99%), 20 wt% Pt/C and sulfur (S, ≥99.5%) were purchased from Aldrich Chemical. Potassium hydroxide solution (KOH, 1.0 M) was bought from Bio-Strategy Laboratory Products Pty Ltd. All chemicals and reagents were commercially available and used as purchased.

S1.2 Preparation of Co_2Cu_1-ONS

Typically, 0.776 g $Co(NO_3)_2·6H_2O$ and 0.322 g $Cu(NO_3)_2·3H_2O$ were dissolved into 50.0 mL deionized water under continuous magnetic stirring for 10 min. Then 20.0 mL $NaBH_4$ solution (0.25 M) was added dropwise, and the solution was further stirred for 5 min. The resulting solid product was centrifuged and washed with absolute ethanol for three times, and finally dried under vacuum for two days. The preparation procedure of Co-ONS was similar to that of Co_2Cu_1-ONS, except that 1.164 g $Co(NO_3)_2·6H_2O$ and 0 g $Cu(NO_3)_2·3H_2O$ were consumed.

S1.3 Preparation of Co_2Cu_1-S

To prepare Co_2Cu_1-S, Co_2Cu_1-ONS (40.0 mg) and S powder (60.0 mg) were placed in two different positions of a porcelain boat and inserted into a tube furnace. The sample was heated at 550 ^oC for 2.0 h with a heating speed of 5.0 ^oC min^{-1} in argon atmosphere, and then cooled down naturally to room temperature. The average yield of Co_2Cu_1-S in five repeated preparation experiments was 20.0±0.5 mg. For comparison, we have also prepared a new Co_2Cu_1-S sample with a smaller S dosage (40.0 mg) at 550 ^oC (Co_2Cu_1-S-2), and another one with the same S dosage (60.0 mg) at a higher temperature (650 ^oC, Co_2Cu_1-S-3). The Co_3S_4 nanonetworks could be prepared via the thermal treatment of Co-ONS with S powder at 550 ^oC.

S1.4 Characterization

X-ray diffraction (XRD) patterns (2θ, 10-70°) were collected on a Bruker D8-Advanced X-ray diffractometer using nickel-filtered Cu-Kα radiation. X-ray photoelectron spectra were obtained by a Kratos Axis ULTRA X-ray photoelectron spectrometer (XPS) with a monochromatic Al Kα (1486.6 eV) radiation at 150 W (15 kV, 10 mA). The binding energies were calibrated using the C 1s peak of adventitious carbon at 284.8 eV as a reference. The thickness values of Co_2Cu_1-ONS and Co_2Cu_1-S were analysed by a Cypher (Asylum Research) atomic force microscope (AFM), whose cantilevers were HA_NC (Etalon) from NT-MDT, having a nominal spring constant of 4.5 N/m and nominal resonant frequency of 145 kHz. Before the AFM test the sample was dissolved in ethanol, centrifuged at 6000 rpm, and the liquid supernatant was diluted by 600 times, then dropped upon the mica plate. Transmission electron microscopy (TEM) and elemental mapping images were obtained by a Tecnai 20 FEG TEM with the acceleration voltage of 200 kV. Co and Cu *K*-edge XAS spectra were recorded on the multipole wiggler XAS beam-line 12 ID in operational mode 1 at the Australian Synchrotron.

S1.5 Electrochemical measurements of thin film electrodes

Thin film electrodes were prepared by dispersing 5.0 mg active catalyst in 0.5 mL ethanol with 50 μL 5 wt% Nafion solution through ultrasonication for 30 minutes. 5 μL of this suspension was drop-cast onto a glassy carbon disk electrode (4 mm diameter, 0.126 cm^2 area) and left to dry naturally. The typical catalyst loading was 0.36 mg cm^{-2}. All the electrochemical tests were performed in a conventional three-electrode system at an electrochemical station (Biologic VMP2/Z multichannel potentiostat), using Ag/AgCl (3 M NaCl) electrode as the reference electrode, graphitic carbon rod as the counter electrode and glassy carbon (GC) electrode as the working electrode. For OER measurement, linear sweep voltammetry with scan rate of 5 mV s^{-1} was conducted in 0.1 M KOH. For ORR measurement, the data were recorded at the scan rate of 10 mV s^{-1}. The rotating speed of the working electrode was increased from 400 to 2500 rpm at the scan rate of 10 mV s^{-1} in O_2-saturated 0.1 M KOH solution during the linear sweep voltammetry test.

S1.6 Zn-air battery test

The performance of the Zn-air battery was tested in a home-built electrochemical cell. Co_2Cu_1-S catalyst was loaded on carbon fiber paper to achieve the mass density of 1.0 mg cm^{-2}, and to function as cathode. Zn plate and 6.0 mol/L KOH aqueous solution were applied as the anode and electrolyte, respectively. All the data were collected on the as-fabricated cell at room temperature. For activity comparison, 20 wt% Pt/C and RuO_2 mixed catalyst was also loaded on carbon fiber paper to function as cathode.

S1.7 Computational methods

Co_3S_4 (311) surface, which is the most exposed surface, was used to build the slab and each slab contained 84 atoms with (1×2) supercell and ~8 Å thickness.

Co_2CuS_4 and Co_2CuO_4 with same crystal structure were used to model the Cu doped materials. A 15 Å vacuum along *z*-direction was applied to prevent unexpected interactions between the periodically repeated images. The atoms in the bottom 3 Å of slabs were fixed in their optimized bulk positons while the others were allowed to relax. All the density functional theory (DFT) calculation was performed using the Vienna Ab initio Simulation Package (VASP) with the generalized gradient approximation (GGA) parameterized by Perdew, Burke and Ernzerhof (PBE) for the exchange correlation functional.[1-3] The kinetic cutoff energy of 500 eV and Gamma k-points of 2×2×1 were used. We select the number of k-point according to a rule of thumb: the product, *k*a* (*k*: the number of k-points; *a*: the length of the basis vector in this direction), should be:

*k*a* ~ 30 Å, for *d* band metals;

*k*a* ~ 25 Å, for simple metals;

*k*a* ~ 20 Å, for semiconductors;

*k*a* ~ 15 Å, for insulators

Considering the length A and B of our models are all larger than 10 Å, we chose the k-points of 2×2×1. The reference information is from https://wiki.fysik.dtu.dk/gpaw/exercises/surface/surface.html.

Besides, all atoms were fully relaxed until the energies and residual forces on each atom converged to 1×10^{-5} eV and 0.02 $eV \cdot Å^{-1}$, respectively. The solvent effects of all calculations were included with an implicit solvation model.[4] The Bader charge analysis was employed to quantitatively describe the charge transfer between the adsorbates and surfaces.[5]

The OER process can be typically described as four electron transfer steps:[6]

$H_2O + * \rightleftharpoons *OH + H^+ + e^-$ (1)

$*OH \rightleftharpoons *O + H^+ + e^-$ (2)

$*O + H_2O \rightleftharpoons *OOH + H^+ + e^-$ (3)

$*OOH \rightleftharpoons * + O_2 + H^+ + e^-$ (4)

where * represents an active site on the catalysts surface, and OH*, O*, OOH* represent three different catalytic intermediates. Based on these four elementary reaction steps, the Gibbs free energy for each step can be obtained by the following expression:[7]

$$G_i(T) = E_{DFT} + G_{correct}(T) + G_U + G_{pH} = E_{DFT} + ZPE - TS + \Delta U_{0\rightarrow T} + G_U + G_{pH} \quad (4)$$

where $G_i(T)$ is the Gibbs free energy at temperature T, E_{DFT} is the DFT energy, $G_{correct}(T)$ is the thermal correction to Gibbs free energy, G_U = eU, U is the electrode potential, $G_{pH} = k_BT\ln10\times pH$. ZPE, S, $\Delta U_{0\rightarrow T}$ are the zero-point energy, entropy and internal energy change induced by temperature respectively. Therefore, the Gibbs free energy change $\Delta G_i(T) = G_i(T) - G_{i-1}(T)$.

The theoretical overpotential η^{OER} and η^{ORR} can be then readily evaluated as:[8]

$$\eta^{OER} = \max(\Delta G_1, \Delta G_2, \Delta G_3, \Delta G_4)/e - 1.23\ V \quad (5)$$

$$\eta^{ORR} = 1.23\ V - \min(\Delta G_1, \Delta G_2, \Delta G_3, \Delta G_4)/e \quad (6)$$

S1.8 DDFT calculations

The established 3D laminated models are solved using the DDFT with finite element method. DDFT describe the time evolution of the one-body density $\rho(\vec{r},t)$ with time t using a continuity equation:

$$\frac{\partial\rho(\vec{r},t)}{\partial t}+\nabla\cdot\vec{J}(\vec{r},t)=0,$$

where the flux $\vec{J}(\vec{r},t)$ is proportional to the gradient of chemical potential:

$$\vec{J}(\vec{r},t)=-\frac{D}{k_BT}\rho(\vec{r},t)\nabla\vec{\mu}$$

with k_B Boltzmann's constant and T the temperature, taken to be 298.15 K. The diffusion coefficients D of the potassium ion, hydroxide ion and oxygen in water were taken to be 1.96×10^{-9} m^2/s, 5.27×10^{-9} m^2/s and 2.42×10^{-9} m^2/s.[9] To achieve the calculations in such complex 3D structure, the excess chemical potential that including hard sphere contribution, van der Waals attraction, Coulomb force and classical correlation term is ignored. Supporting electrolyte assumption was applied for the space representing the electrolyte, in which only diffusion is considered. The flux can be expressed as the gradient of the density of solution species, which is identical to the Fick's law. Together with the continuity equation, we obtain the simple DDFT equation:[10]

$$\frac{\partial\rho(\vec{r},t)}{\partial t}-\nabla\cdot D\nabla\rho(\vec{r},t)=0.$$

The overall OER/ORR reaction in basic solution (0.1 M KOH) is:

$$4OH^{-}\underset{ORR}{\overset{OER}{\rightleftharpoons}}O_2+4e^{-}+2H_2O.$$

The surface reaction is modeled by density-dependent Butler-Volmer correlations to obtain reaction current density:[11]

$$j = j_0 \frac{\rho_i}{\rho_{i,0}} \left[\exp\left(\frac{\alpha_a nF\eta}{RT} \right) - \exp\left(\frac{-\alpha_c nF\eta}{RT} \right) \right]$$

with j_0 is the exchange current density, ρ_i and $\rho_{i,0}$ is the local and bulk density of species i (i = OH^- for OER, and O_2 for ORR), respectively, α_a and α_c is the anodic and cathodic charge transfer coefficients, $n = 4$ is the number of electrons involved in the electrode reaction, F is the Faraday constant, R is the universal gas constant. The bulk concentration of O_2 is considered as 1.2×10^{-3} M in 0.1 M KOH.[12] Generally, in the equation, $\alpha_a + \alpha_c = 1$.[11] The overpotential η is an excess amount of voltage: $\eta = E - E_{eq}$, where E is applied voltage and here $E_{eq} = 1.23$ V for both OER and ORR. The kinetic parameters (α and j_0) for electrode reactions are fitted on the experimental data we obtained using Tafel equation:[13]

$$\eta = \frac{RT}{\alpha nF} \ln j_0 - \frac{RT}{\alpha nF} \ln j$$

Here, for both OER and ORR, the Tafel relations of Co_2Cu_1-S are fitted to obtain the kinetic parameters in the calculations of both Model A and Model B. In OER, α_a = 0.175 and $j_0 = 1.27 \times 10^{-3}$ mA cm^{-2}. In OER, α_c = 0.304 and $j_0 = 6.52 \times 10^{-15}$ mA cm^{-2}. The two models for OER and ORR are simulated by solving the partial differential equation using the COMSOL Multiphysics finite-element-based solver (https://www.comsol.com/). The molar flux of the reactive and produced species at the surfaces are calculated from the current densities using Faraday's law, which is considered as the boundary condition of DDFT. Then, the diffusion layer was established as the result of a dynamic equilibrium between surface reaction and diffusion.

S2 Supporting plots and results

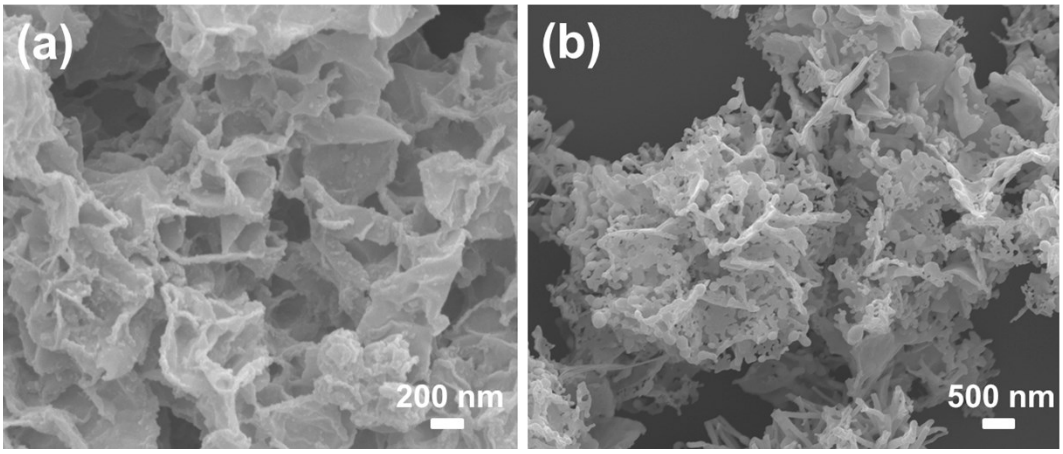

Fig. S1. SEM images of Co_2Cu_1-ONS (a) and Co_2Cu_1-S (b).

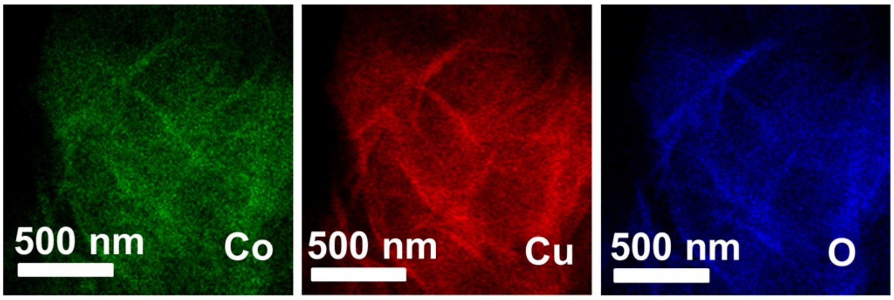

Fig. S2. EDS mapping of Co_2Cu_1-ONS.

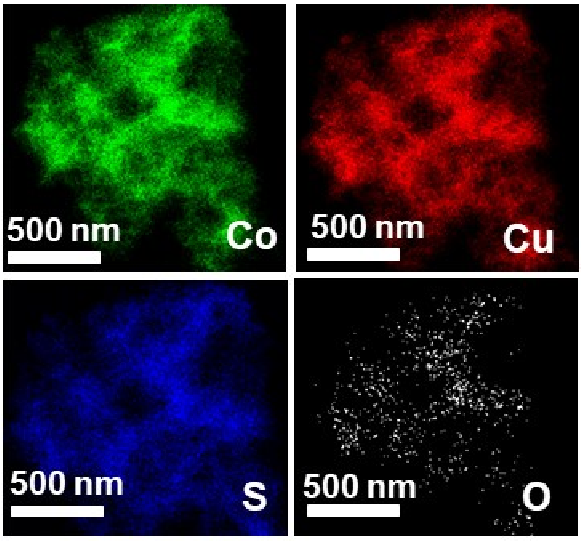

Fig. S3. EDS mapping of Co_2Cu_1-S.

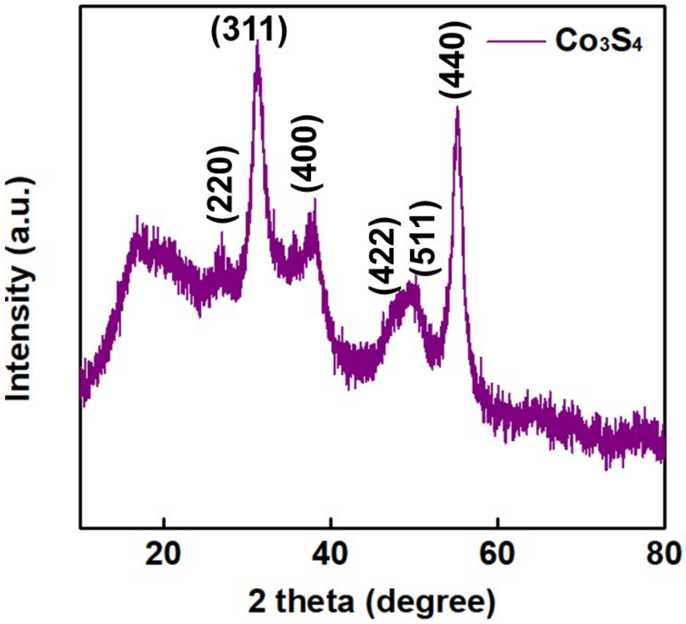

Fig. S4. XRD pattern of Co_3S_4-nanonetworks.

XRD of Co_3S_4 nanonetworks show strong peaks that could be attributed to (220), (311), (400), (422), (511), and (440) planes of cubic Co_2CuS_4 (JCPDS No.47-1738).

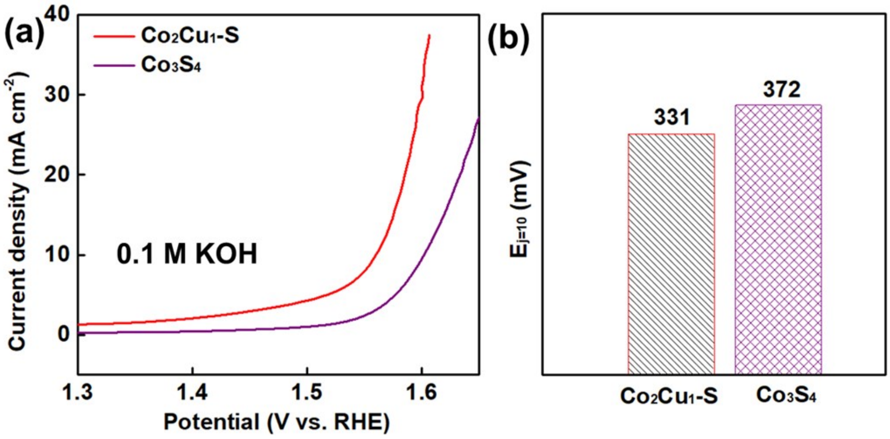

Fig. S5. a) OER polarization curves of Co_2Cu_1-S and Co_3S_4 in 0.1 M KOH, and b) the comparison of their $E_{j=10}$.

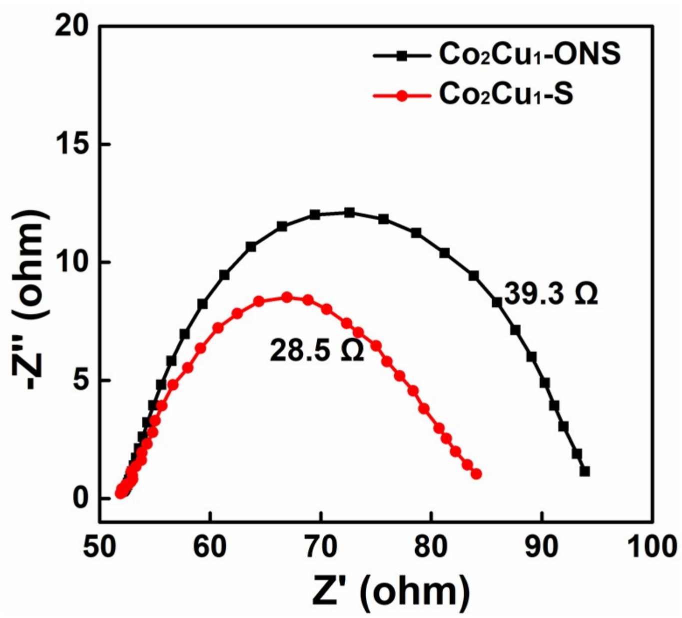

Fig. S6. EIS spectra of Co_2Cu_1-ONS and Co_2Cu_1-S.

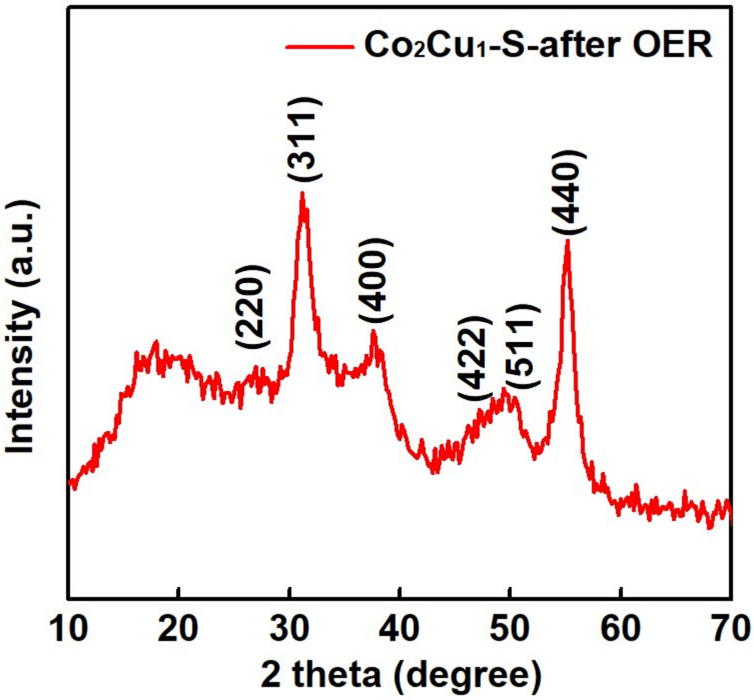

Fig. S7. XRD pattern of Co_2Cu_1-S after OER stability test.

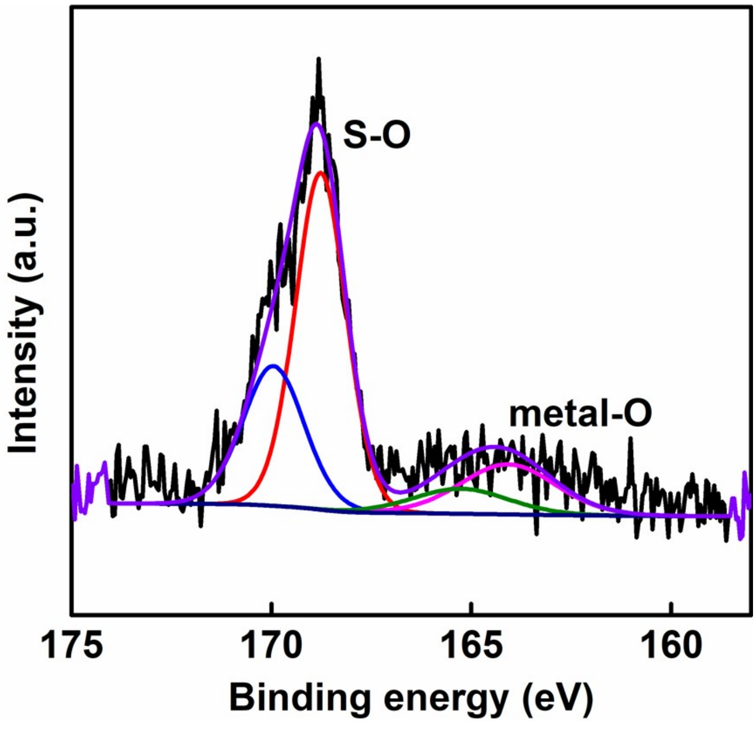

Fig. S8. High-resolution S 2p XPS spectrum of Co_2Cu_1-S after 200000 s stability test.

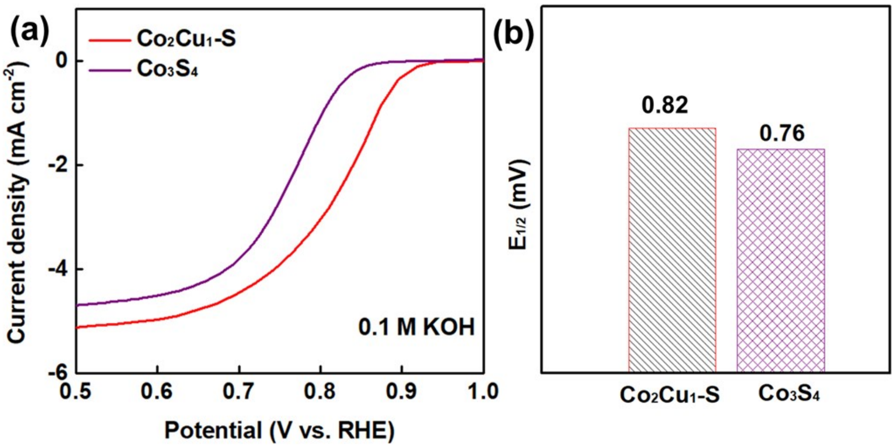

Fig. S9. a) ORR polarization curves of Co_2Cu_1-S and Co_3S_4 in 0.1 M KOH, and b) the comparison of their $E_{1/2}$.

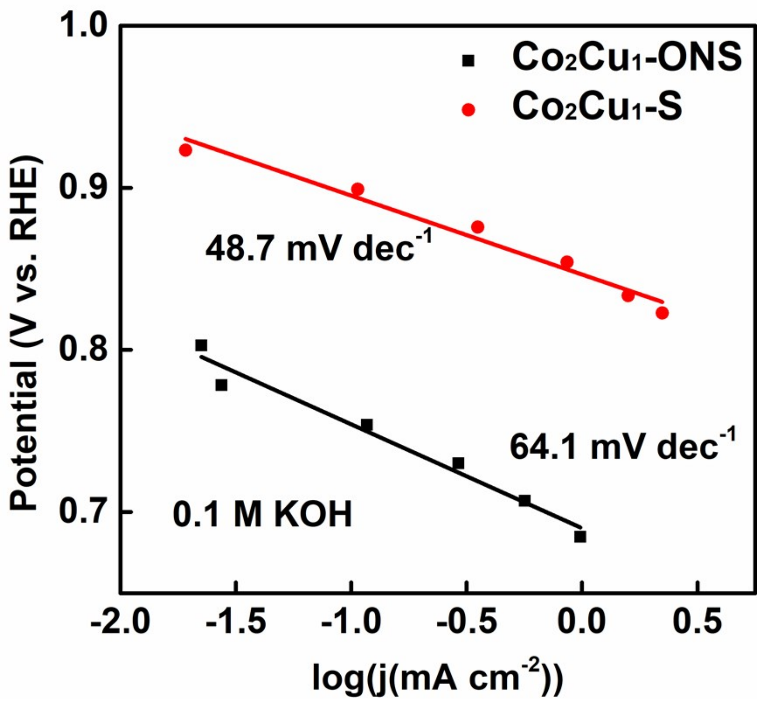

Fig. S10. ORR Tafel plots of Co_2Cu_1-ONS and Co_2Cu_2-S.

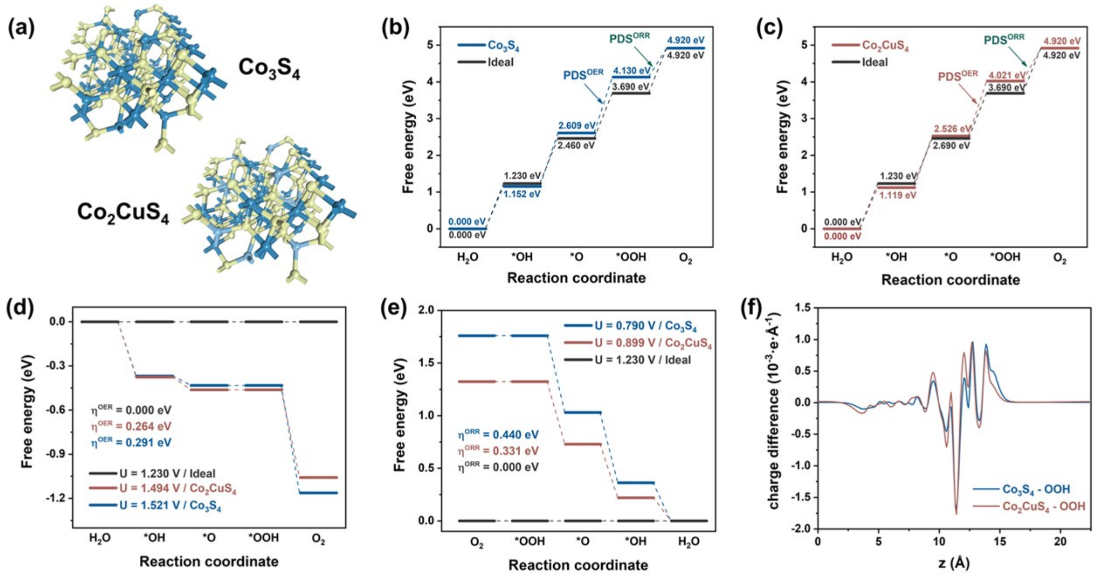

Fig. S11. (a) Surface models of Co_3S_4 and Co_2CuS_4. The standard OER/ORR free-energy profiles of (b) Co_3S_4 and (c) Co_2CuS_4. The blue and green arrows point to the PDSs of OER and ORR, respectively. Energy profiles of Co_3S_4 and Co_2CuS_4 at different potentials and corresponding overpotentials for (d) OER and (e) ORR. (f) Distribution of charge density difference in the direction (*z*) perpendicular to the surface for Co_3S_4 and Co_2CuS_4.

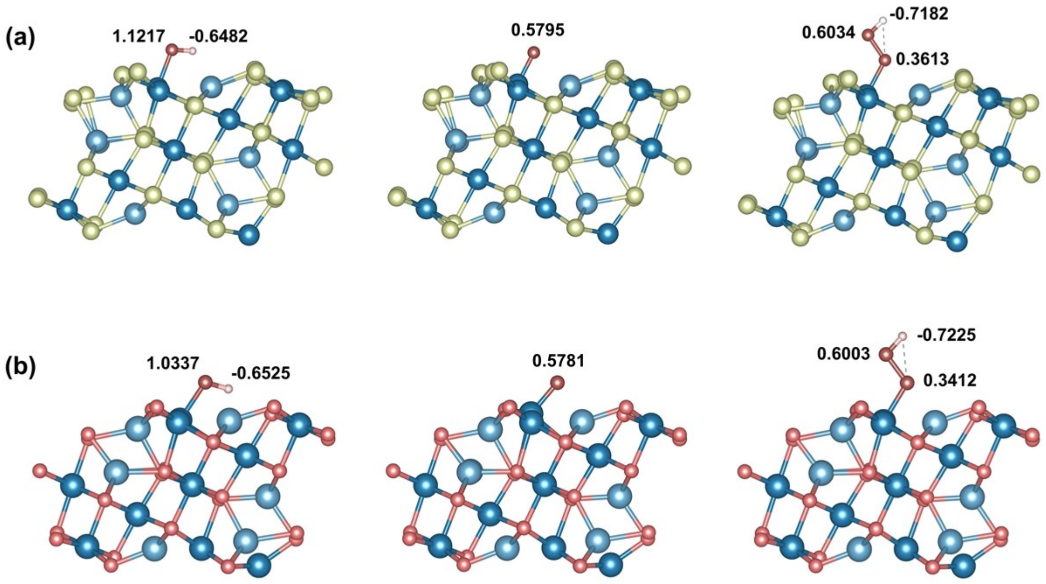

Fig. S12. Bader charge numbers of three adsorbates on the surfaces of (a) Co_2CuS_4

and (b) Co_2CuO_4.

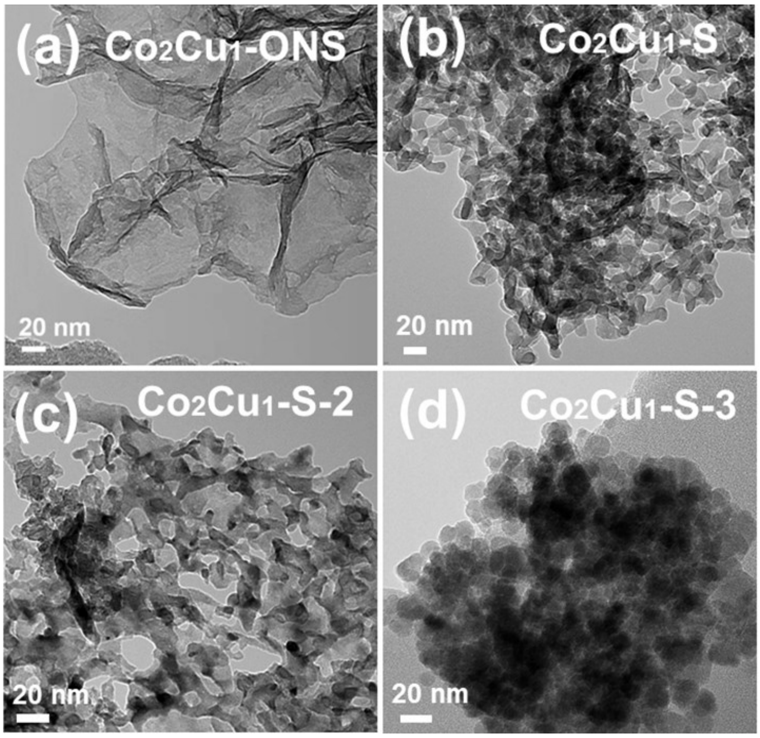

Fig. S13. The SEM images for Co_2Cu_1-ONS, Co_2Cu_1-S, Co_2Cu_1-S-2, and Co_2Cu_1-S-3.

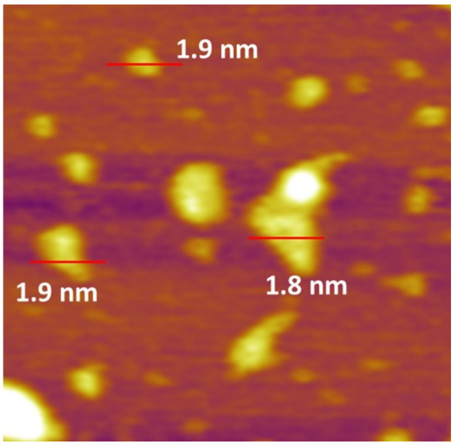

Fig. S14. Atomic force microscopy image of Co_2Cu_1-ONS.

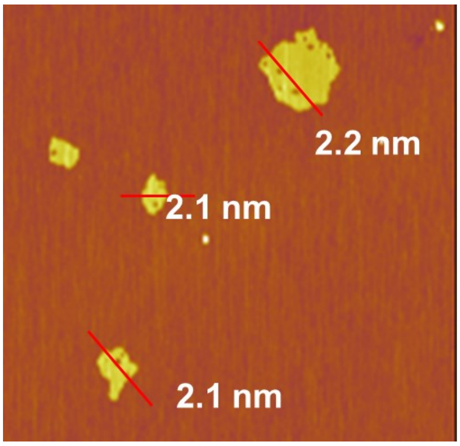

Fig. S15. Atomic force microscopy image of Co_2Cu_1-S.

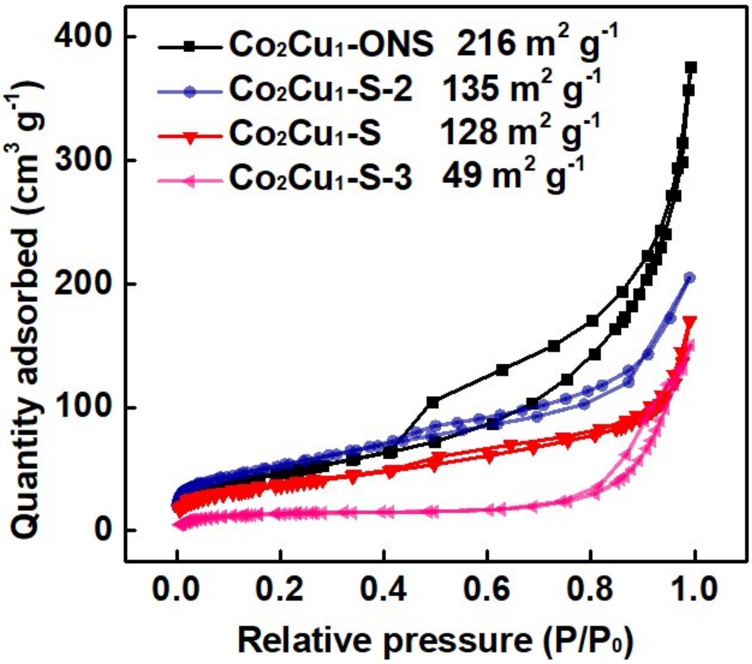

Fig. S16. The BET surface area of Co_2Cu_1-ONS, Co_2Cu_1-S, Co_2Cu_1-S-2, and Co_2Cu_1-S-3.

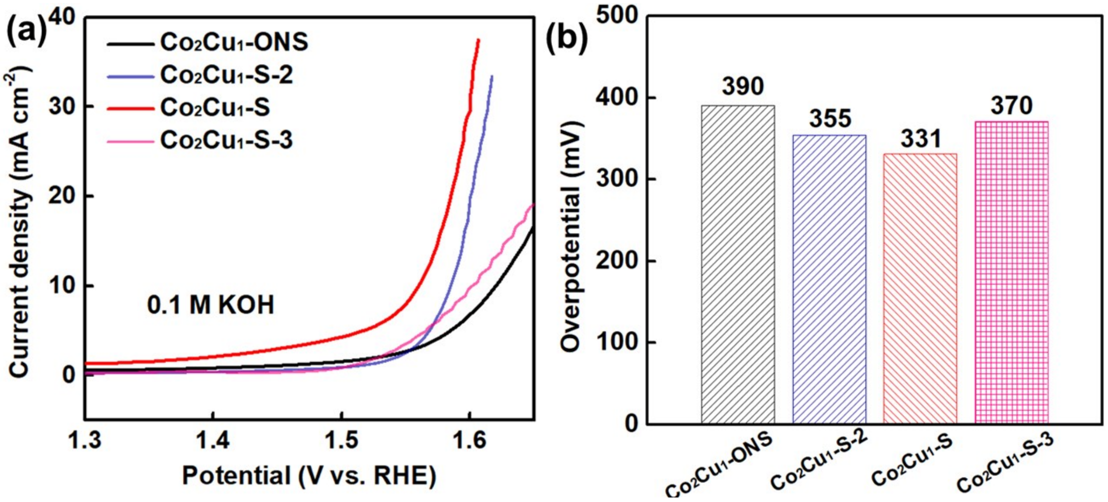

Fig. S17. a) The OER polarization curves of Co_2Cu_1-ONS, Co_2Cu_1-S, Co_2Cu_1-S-2, and Co_2Cu_1-S-3. b) Comparisons of overpotential to reach a current density of 10.0 mA cm^{-2}.

Table R1. Composition of Co_2Cu_1-ONS and Co_2Cu_1-S obtained from ICP-OES.

Sample	Co (wt%)	Cu (wt%)	Molar ratio
Co_2Cu_1-ONS	23.2	12.1	2.05:1
Co_2Cu_1-S	37.9	20.2	2.03:1

References

1. J. F. G. Kresse, *Phys Rev B*, 1996, **54**, 11169-11186.
2. J. F. G. Kresse, *Comput. Mater. Sci.*, 1996, **6**, 15-50.
3. K. B. John P. Perdew, Matthias Ernzerhof, *Phys Rev Lett*, 1996, **77**, 3865-3868.
4. K. Mathew, R. Sundararaman, K. Letchworth-Weaver, T. A. Arias and R. G. Hennig, *J Chem Phys*, 2014, **140**, 084106.
5. G. Henkelman, A. Arnaldsson and H. Jónsson, *Comput. Mater. Sci.*, 2006, **36**, 354-360.
6. J. Rossmeisl, Z. W. Qu, H. Zhu, G. J. Kroes and J. K. Nørskov, *J Electroanal Chem*, 2007, **607**, 83-89.
7. S. S. S. Zuluaga, *J. Chem. Phys.*, 2011, **135**, 134702.
8. I. C. Man, H. Y. Su, F. Calle-Vallejo, H. A. Hansen, J. I. Martínez, N. G. Inoglu, J. Kitchin, T. F. Jaramillo, J. K. Nørskov and J. Rossmeisl, *ChemCatChem*, 2011, **3**, 1159-1165.
9. J. Rumble, *CRC Handbook of Chemistry and Physics*, CRC Press, 100th edn.,

2019.

10. H. Tao, C. Lian and H. Liu, *Green Energy Environ.*, 2020, **5**, 303-321.

11. Allen J Bard, L. R. Faulkner., J. Leddy. and C. G. Zoski., *Electrochemical Methods, Fundamentals & Applications*, Wiley New York, 1980.

12. S. Liu, Z. Li, C. Wang, W. Tao, M. Huang, M. Zuo, Y. Yang, K. Yang, L. Zhang, S. Chen, P. Xu and Q. Chen, *Nat Commun*, 2020, **11**, 938.

13. T. Shinagawa, A. T. Garcia-Esparza and K. Takanabe, *Sci. Rep.*, 2015, **5**, 13801.